Combined Interaction of Phospholipase C and Apolipoprotein A-I with Small Unilamellar Lecithin-Cholesterol Vesicles: Influence of Apolipoprotein A-I Concentration and Vesicle Composition†

Manasa V. Gudheti,‡ Sum P. Lee,§ Dganit Danino,|| and Steven P. Wrenn*,‡

Department of Chemical and Biological Engineering, Drexel University, Philadelphia, Pennsylvania 19104, School of Medicine, University of Washington, Seattle, Washington 98195, and Department of Biotechnology and Food Engineering, Technion, Haifa, Israel 32000

Received December 21, 2004; Revised Manuscript Received March 28, 2005

ABSTRACT: We report the combined effects of phospholipase C (PLC), a pronucleating factor, and apolipoprotein A-I (apo A-I), an antinucleating factor, in solutions of model bile. Results indicate that apo A-I inhibits cholesterol nucleation from unilamellar lecithin vesicles by two mechanisms. Initially, inhibition is achieved by apo A-I shielding of hydrophobic diacylglycerol (DAG) moieties so as to prevent vesicle aggregation. Protection via shielding is temporary. It is lost when the DAG/apo A-I molar ratio exceeds a critical value. Subsequently, apo A-I forms small (∼5−15 nm) complexes with lecithin and cholesterol that coexist with lipid-stabilized (400−800 nm) DAG oil droplets. This microstructural transition from vesicles to complexes avoids nucleation of cholesterol crystals and is a newly discovered mechanism by which apo A-I serves as an antinucleating agent in bile. The critical value at which a microstructural transition occurs depends on binding of apo A-I and so varies with the cholesterol mole fraction of vesicles. Aggregation of small, unilamellar, egg lecithin vesicles (SUVs) with varying cholesterol composition (0−60 mol %) was monitored for a range of apo A-I concentrations (2 to 89 μg/mL). Suppression of aggregation persists so long as the DAG-to-bound-apo A-I molar ratio is less than 100. A fluorescence assay involving dansylated lecithin shows that the suppression is an indirect effect of apo A-I rather than a direct inhibition of PLC enzyme activity. The DAG-to-total apo A-I molar ratio at which suppression is lost increases with cholesterol because of differences in apo A-I binding. Above this value, a microstructural transition to DAG droplets and lecithin/cholesterol A-I complexes occurs, as evidenced by sudden increases in turbidity and size and enhancement of Förster resonance energy transfer; structures are confirmed by cryo TEM.

Molecular details concerning nucleation of cholesterol monohydrate crystals in the context of gallstone pathogenesis are largely lacking. Few measurements of cholesterol nucleation kinetics are available (*1*, *2*), and fundamental questions about the nucleation mechanism remain unanswered. For example, what is the critical cluster size? Does nucleation proceed within the bilayer or in the surrounding aqueous phase? Historically, studies examining cholesterol nucleation in bile have appealed to a concept of "nucleation time," introduced by Holan (*3*) and defined as the time at which cholesterol monohydrate crystals first appear in an optical microscope (that is, seen by light microscopy). The nucleation time does not yield information on nucleation per se, because nucleation events are largely completed by the time crystals can be detected. Nonetheless, the method was useful to identify "pro-" and "antinucleating factors" (PNFs[1] and ANFs, respectively), so named because of their influence on nucleation time relative to a control sample (*4*). PNFs and ANFs are typically but not always proteins or enzymes. PNFs include phospholipase C (PLC) (*5*), immunoglobulins (*6*), fibronectin (*7*), concanavalin A-binding nonmucous glycoproteins (*8*), mucous glycoproteins (*9*), and aminopeptidase N (*10*), and the most commonly reported ANFs are apolipoprotein A-I (apo A-I) and apolipoprotein A-II (*11*−*13*).

There is a great deal of interest in PNFs and ANFs because of the direct dependence of gallstone formation on the rate of cholesterol nucleation from cholesterol-rich vesicles (*14*−*16*). It is widely held that knowledge of the mechanisms by which PNFs and ANFs alter cholesterol nucleation kinetics will be a key to preventing gallstone formation in humans (*16*). While this might be true, one must remain mindful that abundance of a single PNF or deficiency of a single ANF in itself is unlikely to determine the incidence of stones. A more

† This work was supported in part by a Biomedical Engineering Research Grant from the Whitaker Foundation (RG-00-0417).

* To whom correspondence should be addressed. Telephone: +1-215-895-6694. Fax: +1-215-895-5837. E-mail: wrenn@coe.drexel.edu.

‡ Drexel University.

§ University of Washington.

|| Technion.

[1] Abbreviations: ANF, anti-nucleating factor; apo A-I, apolipoprotein A-I; CH, cholesterol; Cryo-TEM, cryogenic transmission electron microscopy; DAG, diacylglycerol; DHE, dehydroergosterol; DL, dansylated lecithin; DLS, dynamic light scattering; EDTA, ethylene diamine tetraacetic acid; FRET, Förster resonance energy transfer; HDL, high-density lipoprotein; L, egg-yolk lecithin (phosphatidylcholine); LDL, low-density lipoprotein; PNF, pronucleating factor; SUV, small unilamellar vesicle.

10.1021/bi047317m CCC: $30.25
Published on Web 04/21/2005

likely scenario is that stone formation is governed by a combination of factors, including interactions between multiple PNFs and ANFs. To date, such interactions have not been fully explored.

As a first attempt to investigate interactions between PNFs and ANFs, we recently described the combined effects of PLC and apo A-I in solutions of model bile (*11*). PLC is a well-studied enzyme that cleaves the phosphoester bond of phosphatidylcholine on the outer leaflet of lecithin-cholesterol vesicles, thereby eliminating polar phosphocholine headgroups and generating hydrophobic diacylglycerol (DAG) moieties within the lipid bilayer (*1*). Strictly speaking, PLC is not a pronucleating factor but rather a proaggregating factor. That is, PLC induces vesicle aggregation so as to eliminate (hydrophobic) exposure of DAG to water (*1*, *17*). Indirectly, PLC is pronucleating because vesicle aggregation enhances nucleation (*18*); we believe this is because aggregation facilitates collisions of either cholesterol-rich (liquid-ordered) domains known to exist in phosphatidylcholine bilayers (*19*, *20*) or putative, cholesterol-pure (nano) domains recently described in both model (*21*−*23*) and native (*24*) membranes or both.

Apo A-I is a 243 amino acid, 28-kDa amphipathic, helical protein that constitutes the major protein component of high-density lipoprotein (HDL) (*25*). Apo A-I resides on the surface of HDL and stabilizes exposed hydrophobic surfaces and also facilitates the solubilization of hydrophobic lipids in blood (*26*). Apo A-I is also known to transform phospholipid bilayer vesicles into smaller discoidal complexes (*27*). Two models of apo A-I structural organization in phospholipid disc complexes have been proposed: (i) picket fence model (*28*), in which the apo A-I helical segments are organized parallel to the acyl chain, and (ii) belt model (*29*), in which the helical segments are perpendicular to the acyl chains.

Relevant to this work, both PLC and apo A-I are present in bile, where they act as PNF and ANF, respectively. PLC, secreted by gallbladder epithelial cells, has been identified in bile with activity levels ranging from 1 to 123 nmol h^{-1} mg^{-1} (*30*, *31*). Likewise, apo A-I has been found to prolong nucleation time in model bile systems (*12*, *13*, *32*). The concentration of apo A-I in human bile ranges from 20 to 320 μg/mL (*12*).

A key finding of the initial PLC/apo A-I study was that apo A-I prevents PLC-induced vesicle aggregation via two mechanisms. One is "shielding" of DAG moieties, whereby apo A-I intercalates into the membrane so as to cover DAG and eliminate its exposure to water. If and when the surface area of exposed DAG exceeds the amount that can be covered by apo A-I, then shielding is rapidly lost. A sudden and extensive rise in sample turbidity ensues, which we attribute to a microstructural transition to relatively large (400−800 nm) DAG-rich oil droplets and relatively small (∼15 nm) lecithin/cholesterol/apo A-I complexes. We contend that this microstructural transition constitutes a second (newly discovered) mechanism by which apo A-I inhibits cholesterol nucleation in bile.

A noteworthy observation from the initial PLC/apo A-I study was that the microstructural transition occurred only in cholesterol-enriched systems; shielding persisted for the duration of the experiment in cholesterol-free systems. We do not interpret this to mean cholesterol is necessary for complex and DAG droplet formation. Rather, we hypothesize that a microstructural transition is a general phenomenon that can (and does) happen at any cholesterol mole fraction. The discrepancy between cholesterol-free and cholesterol-enriched behavior observed previously is easily explained by the fact that cholesterol impedes apo A-I binding to phospholipid bilayers (*33*). If a transition to complexes and droplets does not occur until the molar ratio of DAG to bound apo-A-I exceeds a critical value, corresponding roughly to the molecular surface area ratio of DAG to apo A-I (∼1:100), then increasing the cholesterol mole fraction should require a higher total concentration of apo A-I to achieve shielding for a given period of time. As stated another way, if the total apo A-I concentration is held constant, then the time at which shielding is lost and a microstructural transition occurs should decrease with increasing cholesterol content.

The present study seeks to test this hypothesis and to confirm and build on the findings of the initial PLC/apo A-I study (*11*). In particular, we demonstrate that the loss of shielding is indeed possible in cholesterol-free systems provided that the apo A-I concentration is sufficiently low. More generally, we provide an exhaustive study of PLC/apo A-I interactions in model bile over a range of apo A-I concentrations (2−89 μg/mL), cholesterol mole fractions (0−60 mol %), and total lipid concentrations (0.82 and 6.52 mM). Estimates of apo A-I binding constants as a function of cholesterol mole fraction are provided, and predictions based on these estimates are compared with experimental results. Shielding against vesicle aggregation is monitored during DAG formation by measuring changes in sample turbidity. Dynamic light scattering (DLS) is used to determine sizes of both vesicle aggregates and DAG oil droplets; the identity of scattering structures, vesicles, or DAG oil droplets is visualized via cryo-transmission electron microscopy (Cryo-TEM). Finally, Förster resonance energy transfer (FRET) from dehydroergosterol (DHE) to dansylated lecithin (DL) is used to identify complex formation and confirm the onset of a microstructural transition.

EXPERIMENTAL PROCEDURES

Sample Selection: Lipid Concentrations. Here, we are interested in PLC and apo A-I interactions with biliary lecithin-cholesterol vesicles. Neglecting bile salts, because they are not components of vesicles, native human gallbladder bile concentrations of lecithin plus cholesterol range from 13.5 to 87.5 mM (*18*, *34*). While we wish to achieve physiological relevance to the greatest extent possible and would therefore prefer to make model bile solutions in the native concentration range, experimental constraints must also be considered.

For example, excessive sample turbidity leads to artifactual attenuation of fluorescence intensities via the well-known inner filter effect (*35*). Similarly, excessive turbidity can lead to interparticle interactions and multiple scattering, which complicates DLS analyses. Given the use of PLC in this work, which enhances the extent of vesicle aggregation significantly, lipid concentrations that match physiological conditions become impractical. Two lipid concentrations are employed herein, one for turbidity and DLS measurements (nominally 0.8 mM) and one for fluorescence spectroscopy measurements (nominally 6.5 mM). It is noted that the latter

value approaches the lower end of the physiological range. Moreover, the work is deemed applicable to *in vivo* systems wherein higher lipid concentrations and other factors are expected to influence some of the details but not the underlying phenomena driven by physical chemistry, being investigated.

Apo A-I Concentrations. The apo A-I concentrations used in this work (2−89 μg/mL) fall largely within the physiological range (20−320 μg/mL). Apo A-I concentrations that are slightly less than physiological values are used for two reasons. One is to maintain a physiological ratio of apo A-I to total lipids, bearing in mind that the total lipids concentration is less than physiological for reasons previously discussed. A second reason is to test the hypothesis that complex formation and a concomitant microstructural transition to DAG oil droplets are not unique to cholesterol-containing liposomes. Accordingly, the apo A-I concentration is decreased steadily in cholesterol-free systems, without regard to physiological values, to determine whether a *de minimus* level exists, below which protection via shielding is lost.

PLC Concentration. The level of PLC activity in human bile varies over a wide range (1−123 nmol mg^{-1} h^{-1}) (*30*). For purposes of experimental investigation, it has been found that commercially available bacterial phospholipase C (*Clostridium perfringens*) produces changes nearly identical to that of the partially purified native enzyme (*31*). Although the concentrations of PLC in human bile are not reported, the concentrations used herein are consistent with earlier studies. Perhaps more important than the PLC enzyme concentration is the relative enzyme-to-vesicle ratio; that value is approximately unity (although the exact value varies somewhat with vesicle size and composition).

Analytical Approach. The model systems to be studied include small, unilamellar, lecithin-cholesterol vesicles prepared by sonication and exposed to various combinations of PLC and apo A-I. The extent to which the vesicles aggregate is quantified in terms of turbidity by measuring absorbance at 450 nm. Absorbance is a misnomer in this sense, because nothing in the samples literally absorbs the incident radiation. Rather, the intensity of incoming light is attenuated because of scattering, and this is registered as absorbance using an ultraviolet/visible spectrometer. Turbidity values are calculated from the measured absorbance values based on a path length of 1.1 cm. An alternative for measuring aggregation is to record light scattering intensity, but absorbance is the preferred method for the highly turbid samples used herein.

DLS is used here to measure "particle" sizes. In these studies, the term particle refers to any of the following entities, depending on which causes the scattering: a single vesicle, a group of aggregated vesicles, a lecithin/cholesterol/apo A-I complex, apo A-I alone, or a DAG oil droplet. An upturn in absorbance and a concomitant increase in particle size could result from either vesicle aggregation or DAG oil droplet formation or both. Cryo-TEM is employed both to confirm the sizes measured with DLS and to confirm the identification of any structures present. Because complexes are sufficiently small so as to be possibly obscured during DLS measurements, a FRET assay is used as an additional test of complex formation.

Additional studies include: (1) measuring spectral shifts of DL, a fluorescent analogue of native lecithin, to determine whether apo A-I interferes with PLC hydrolysis of lecithin and (2) use of ethylenediamine tetraacetic acid (EDTA) to chelate calcium and determine whether such "quenching" of PLC prevents eventual loss of shielding against aggregation. Details of sample preparation and analytical methods appear below.

Materials. Egg yolk lecithin (L), cholesterol (CH), dehydroergosterol (ergosta-5,7,9(11),22-tetraen-3b-ol) (DHE), NaCl, $CaCl_2$, HEPES, NaN_3, Na_2EDTA (disodium ethylenediamine tetraacetic acid), and PLC of highest purity from *C. perfringens* were purchased from Sigma−Aldrich Co. (St. Louis, MO). Apo A-I of >95% purity from human plasma was purchased from Calbiochem (La Jolla, CA) and used without further purification. Dansylated lecithin (1-acyl-2-[12-[(5-(dimethylamino)-1-naptalenesulfonyl)amino]dodecanoyl]-*sn*-glycero-3-phosphocholine) (DL) was custom-synthesized by Avanti Polar Lipids, Inc. (Alabaster, AL). Reagents (methanol and chloroform) of analytical grade were purchased from Fisher Scientific (Suwanee, GA). All lipids and chemicals were used without further purification. All glassware was acid-washed, and water used in sample preparation was both distilled and deionized. The experiments were performed at room temperature.

Sample Preparation. Stock solutions of L, CH, and DHE were dissolved separately in chloroform to give final concentrations of 100, 100, and 5 mg/mL, respectively. DL was dissolved in methanol to yield a stock solution concentration of 5 mg/mL. Mixtures of CH, L, DHE, and DL were coprecipitated from chloroform to give lipid films of desired composition. The mixing was done in 20 mL scintillation vials, and the solvent was removed under a stream of nitrogen in a rotary evaporator. The films were then placed in a vacuum oven at room temperature and vacuum of 28 inches of Hg for 24 h. After solvent removal, the lipid films were hydrated with the appropriate amount of buffer (0.15 M NaCl, 5 mM $CaCl_2$, 5 mM HEPES, and 0.02 wt % NaN_3 at pH 7.4) and vortex-mixed for 5 min followed by direct bath sonication (Misonix, Inc., Farmingdale, NY, Ultrasonic Processor XL2020) for 90 min. Sonicated dispersions were centrifuged at 32000*g* and 15 °C for 90 min (Beckmann Coulter Allegra 64R), and the supernatant was filtered (0.22 μm Millipore) and diluted with buffer solution to yield unilamellar vesicles at the desired overall lipid concentration.

Aliquots (3 mL) from a vesicle solution of the desired composition were pipetted into quartz cuvettes. PLC alone, apo A-I alone, or PLC plus apo A-I were added (experimental samples), or nothing was added (control sample) to the vesicle aliquots. When used together, apo A-I was always added prior to PLC. The stock solution of PLC used was 2 units/mL. Vesicles used in the fluorescence studies contained DHE alone, DL alone, or both DHE and DL. DHE accounted for 17.5 mol % of the total sterol, and DL constituted 3 mol % of the total lecithin, in the fluorescent samples. The total lipid concentration was nominally 0.8 mM in nonfluorescent samples and 6.5 mM in fluorescent samples. Where Na_2EDTA, a calcium-chelating agent, was used, 200 μL of a 0.31 M solution was added to a vesicle aliquot at 3 min to deactivate PLC hydrolysis.

Absorbance Spectroscopy. Absorbance at 450 nm was used to quantify particle aggregation. Absorbance was measured using a Perkin−Elmer Lambda 40 UV−vis spectrometer (Shelton, CT). Values are reported in terms of turbidity, τ,

because light attenuation was caused by light scattering and not genuine absorbance. The relationship between turbidity and absorbance (Abs) is

$$\tau = 2.303\text{Abs}/l \quad (1)$$

where l is the path length of the sample through which light passes.

Dynamic Light Scattering (DLS). The autocorrelation function of light scattering intensity provided a measure of particle sizes and polydispersities. Particle sizes were analyzed using a Brookhaven 90Plus DLS apparatus (Holtsville, NY). This system consists of a 15 mW, solid-state laser operating at a 678 nm wavelength and a BI-9000AT digital autocorrelator. The measured autocorrelation functions were analyzed for the first and second cumulants of a cumulant fit, which provide measures of the apparent diffusivity and polydispersity, respectively. Sizes are reported in terms of an effective diameter, calculated from the Stokes−Einstein equation

$$\text{effective diameter} = k_B T/3\pi\nu D \quad (2)$$

where k_B is the Boltzmann constant, T is the temperature (25 °C), ν is the solvent viscosity, and D is the diffusivity from the first cumulant.

Fluorescence Spectroscopy. Steady-state fluorescence measurements were made using a model A-710 fluorescence spectrometer from Photon Technology International, Inc. (Ontario, Canada) with the band-pass set to 2 nm. The fluorescent probes used were DHE and DL, fluorescent analogues of the native lipids, cholesterol and lecithin, respectively. The excitation wavelength was set at 300 nm. The emission spectra of DHE and DL were measured from 325 to 550 nm and subsequently smoothed using the Savistsky and Golay method (*36*). DHE emission intensity at 372 nm and DL maximal intensity were obtained from the smoothed spectra.

Cryogenic Transmission Electron Microscopy (Cryo-TEM). Solutions were prepared at 25 °C in the controlled environment vitrification system (CEVS), at 100% relative humidity to avoid evaporation of water and structural changes during specimen preparation (*37*). Specimens were prepared on 400 mesh copper grids coated with a perforated formvar film (Ted Pella). Briefly, a small drop (∼8−10 μL) was applied onto the grid and blotted with a filter paper to form a thin liquid film of solution, 100−250 nm in thickness. The blotted sample was immediately plunged into liquid ethane at its freezing point (−183 °C), and the resulting vitrified specimen was transferred into liquid nitrogen (−196 °C) for storage. Samples were examined in a Philips CM120 transmission electron microscope (TEM), operated at 120 kV, using an Oxford 3500 cryo-holder maintained at below −178 °C or with a 2000 FX JEOL TEM, at 100 kV, with a Gatan 626 cold stage maintained at below −168 °C. Images were recorded digitally on a Gatan 791 MultiScan cooled charge-coupled device (CCD) camera with the Digital Micrograph 3.1 software package. Microscope magnifications were in the range of 10 000−175 000, equivalent to real image magnifications of up to 47 000. Images were acquired at nominal defocus of 4−7 μm to enhance phase contrast and at low dose conditions to minimize electron beam radiation damage, using imaging procedures developed specifically for morphological studies (*38*). Brightness and contrast enhancement were done using the Adobe Photoshop 7.0 ME package.

Enzyme Kinetics Model. A kinetic model for PLC enzyme kinetics based on a modified version of the classical Michaelis−Menten model is used to compute DAG concentrations as a function of time (*1*). The modified model accounts for PLC inhibition by DAG, which seemingly competes with lecithin as a substrate for PLC. A two-step mechanism best describes the kinetics of PLC hydrolysis in lecithin-cholesterol vesicles: first is production of DAG according to the traditional Michaelis−Menten framework, described by a maximal rate, V_{max}, a total enzyme concentration $[PLC]_T$, a first-order rate constant, k_2, and a Michaelis constant, K_M; second is an irreversible binding between DAG and PLC to account for observed inhibition of PLC activity. This binding is modeled as a second-order process with rate constant k_3. Values for model parameters are $\{V_{max}/[PLC]_T\} = k_2 = 1000\ \text{min}^{-1}$, $K_M = 2.0$ mM, and $k_3 = 0.035$ (mM min)$^{-1}$. This model was developed and used previously to describe PLC kinetics in model bile systems (*1*).

RESULTS

Behavior of Cholesterol-Enriched SUVs. Figure 1a depicts the turbidity, measured as absorbance at 450 nm, for a cholesterol-enriched (60% sterol) system. The total lipid concentration was fixed at 0.815 mM, and the concentration of PLC, when present, was 0.2 unit. Results depend largely on the presence and concentration of apo A-I. In the absence of PLC, apo A-I does not induce any increase in turbidity. In comparison with a control sample containing no apo A-I or PLC, the only effect of apo A-I is a modest suppression of turbidity. On the other hand, PLC alone induces a steady increase in turbidity over the 7 h period studied. When apo A-I is present with PLC, the turbidity behavior varies in a dose-dependent fashion. For apo A-I concentrations greater than or equal to 23 μg/mL, there is an initial suppression of turbidity, compared with the control, followed by an increase in turbidity that is ∼3 times larger than that observed with the control. Apo A-I concentrations less than 23 μg/mL also give an increase in turbidity ∼3 times greater than the control but without the initial suppression. The lines are drawn as a visual aid to depict the absorbance profiles for different sample conditions.

Figure 1b depicts the changes in effective diameters of the SUVs as measured by DLS and are complimentary to the absorbance profiles in Figure 1a. Apo A-I alone does not induce any change in vesicle size, as evidenced by the fact that effective diameter remains ∼100 nm throughout the 7 h experiment. A similar statement applies to the control sample. PLC alone induces a steady aggregation of SUVs, as revealed by an increase in size from an initial value of ∼100 nm to a final value of ∼300 nm. When apo A-I is present with PLC, the final size varies between 400 and 800 nm for the range of apo A-I concentrations studied (2−84 μg/mL). Temporary suppression of vesicle aggregation is observed for the first 30 min in samples containing 46 and 84 μg/mL apo A-I, but samples with apo A-I concentrations less than 46 μg/mL do not exhibit this suppression. After 7 h, the effective diameter in all samples containing PLC plus apo A-I is greater than that exhibited by the sample

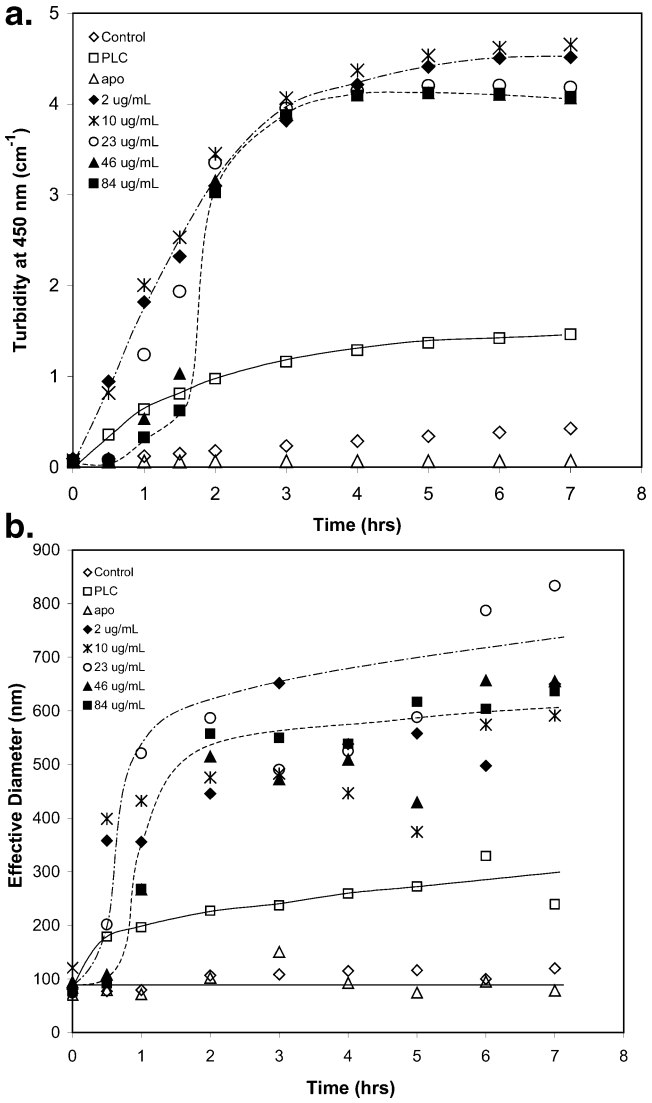

FIGURE 1: Turbidity (a) and effective diameter (b) of cholesterol-enriched SUVs (60% sterol) in the presence of PLC and varying apo A-I concentrations. Turbidity at 450 nm and effective diameter (nm) are plotted versus time for SUVs (0.815 mM total lipid concentration) containing PLC (0.2 unit) and a range of apo A-I concentrations (2−84 μg/mL). The control consists of SUVs devoid of PLC and apo A-I. The "PLC" (□) and "apo" (△) samples consist of PLC (0.2 unit) and apo A-I (46 μg/mL) alone, respectively. Other samples contained 0.2 unit of PLC plus the amount of apo A-I indicated in μg/mL. Apo A-I alone (△) behaves like the control (◇). PLC alone (□) induces a steady increase in turbidity. The presence of apo A-I in conjunction with PLC induces an increase in turbidity greater than that observed in the "PLC" sample. The samples containing apo A-I with concentrations greater than or equal to 26 μg/mL experience suppression in turbidity initially, with the length of the lag period being proportional to the apo A-I concentration. PLC alone (□) induces SUV aggregation from an initial value of ∼100 to ∼300 nm at the end of 7 h. The presence of apo A-I leads to SUV aggregation greater than that observed with PLC alone, with sizes ranging from ∼400 to ∼800 nm. With the two highest apo A-I concentrations employed, a lag period is observed in both the turbidity and size profiles. The lines shown in the figures are drawn as a guide to the eye. Different lines (— and ⋯) are used to distinguish various sample conditions.

containing only PLC ("PLC alone "). Lines are drawn as an aid to the eye to show effective diameter profiles for different sample conditions.

Behavior of Cholesterol-Free SUVs. Figure 2a shows the turbidity for cholesterol-free SUVs exposed to the same range

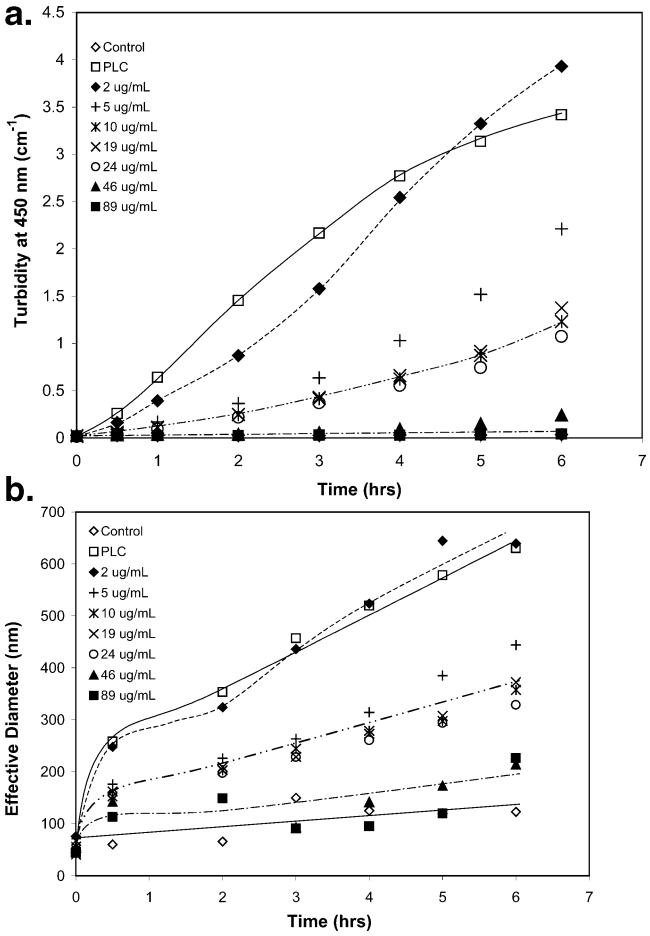

FIGURE 2: Turbidity (a) and effective diameter (b) of cholesterol-free lecithin-only SUVs (0% sterol) in the presence of PLC and varying apo A-I concentrations. Turbidity at 450 nm and effective diameter is plotted versus time for SUVs (0.815 mM total lipid concentration) containing PLC (0.2 unit) and a range of apo A-I concentrations (2−89 μg/mL). The control (◇) consists of SUVs devoid of PLC and apo A-I. The "PLC" (□) and "apo" (△) samples consist of PLC (0.2 unit) and apo A-I (46 μg/mL) alone, respectively. Other samples contained 0.2 unit of PLC plus the amount of apo A-I indicated in μg/mL. The total lipid, PLC, and apo A-I concentrations are the same as the 60% sterol SUVs in Figure 1. Unlike the cholesterol-enriched SUV system, the two highest apo A-I concentrations completely suppress the PLC-induced vesicles aggregation as seen by the flat turbidity profiles that resemble the control. Only the turbidity of the lowest apo A-I concentration (2 μg/mL) exceeds that of the "PLC" sample. Apo A-I dose-dependent decrease in turbidity and size is observed. Higher apo A-I concentrations give rise to lower turbidity values and smaller size particles. The lag period observed varies with the apo A-I concentration in a dose-dependent fashion. The SUV size distribution varies from ∼200 to ∼650 nm at the end of 7 h. Lines are drawn as a visual aid, and the different types of lines are used to distinguish sample conditions.

of apo A-I concentrations as in the cholesterol-enriched system (Figure 1). The cholesterol-enriched and cholesterol-free SUVs have the same total lipid concentration (0.815 mM) and the same PLC concentration (0.2 unit). Similar to the cholesterol-enriched systems, complete suppression is temporary, for a limited number of apo A-I concentrations (5−24 μg/mL), and turbidity eventually increases (after 1 h). Unlike the cholesterol-enriched SUVs, the two highest apo A-I concentrations employed suppress the PLC-induced increase in turbidity for the duration of the experiment. Only the lowest apo A-I concentration (2 μg/mL) induces a

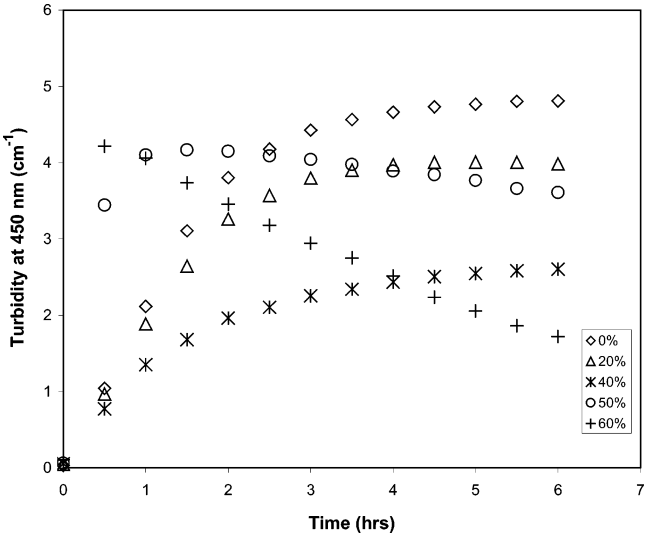

FIGURE 3: PLC-induced aggregation of SUVs with varying cholesterol mole percentage. Turbidity at 450 nm is monitored as a function of time for SUVs with cholesterol mole percentages of 0, 20, 40, 50, and 60% to which PLC (0.2 unit) was added to induce enzyme action. The total lipid concentration is the same in all samples (0.815 mM), with the lecithin concentration is decreasing as a function of increasing cholesterol content. The 0% (◇), 20% (△), and 40% (*) samples show turbidity profiles that mirror the lecithin concentration in the system. At the two highest cholesterol contents investigated, 50% (○) and 60% (+), despite the lower substrate concentration (lecithin), a rapid rise in turbidity followed by a decline is observed.

turbidity value greater than that observed in the PLC-alone sample after 6 h.

Figure 2b shows the effective diameters for the samples in Figure 2a. The control sample, which contains neither apo A-I nor PLC, exhibits a constant effective diameter (∼100 nm). The PLC-alone sample exhibits a steady increase in size from an initial value of ∼100 nm to a final value of ∼650 nm after 6 h. The effective diameter of the samples containing both apo A-I and PLC depended on the apo A-I concentration employed. The lowest apo A-I concentration (2 μg/mL) induced an approximately 6- to 7-fold increase in size (from ∼100 nm to ∼650 nm), whereas the highest apo A-I concentration (89 μg/mL) caused only a doubling in size (from ∼100 to ∼200 nm). Intermediate apo A-I concentrations induced intermediate size changes. Lines are again drawn as visual aids to depict the profiles for various sample conditions.

PLC-Induced Aggregation of SUVs with Varying Cholesterol Mole Percentage. Because cholesterol is known to promote vesicle aggregation, a control study was performed to show the influence of cholesterol on PLC-induced vesicle aggregation.

Figure 3 shows turbidity profiles for SUVs with varying cholesterol mole percentages. A total of 0.2 unit of PLC was added to 3 mL aliquots of varying vesicle compositions. All SUVs have the same lipid concentration (0.815 mM) so that the lecithin concentration decreases with increasing cholesterol mole percentage. For the 0, 20, and 40% SUVs, turbidity decreases in a substrate (lecithin) dose-dependent fashion. This is an important result, because it shows that the amount of substrate is the dominant factor in determining aggregate size up to 40 mol % cholesterol; not until the vesicle cholesterol composition reaches 50−60% do higher cholesterol values give larger amounts of aggregation.

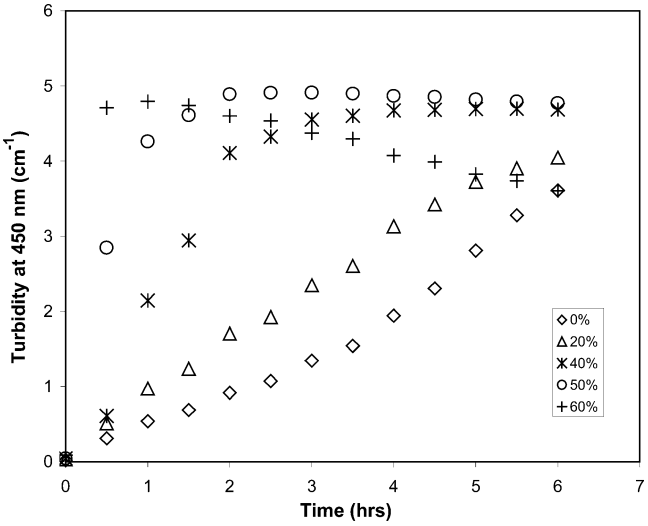

FIGURE 4: Effect of vesicle composition on the turbidity profile of SUVs at a low apo A-I concentration (19 μg/mL). A total of 0.2 unit of PLC and 19 μg/mL apo A-I were added to SUVs (0.815 mM total lipid concentration) of varying cholesterol contents. The rise in turbidity is proportional to the cholesterol content of the SUVs. Initial suppression in turbidity is not observed in any of the samples.

SUV Aggregation Profile at a Low (19 μg/mL) Apo A-I Concentration. Figure 4 shows results obtained when the turbidity study of Figure 3 is repeated in the presence of apo A-I. Again, 3 mL aliquots of SUVs of varying cholesterol mole percentages were exposed to 0.2 unit of PLC but also to 19 μg/mL apo A-I. In this case, turbidity increases with cholesterol composition for the entire cholesterol composition range. This is in contrast to Figure 3, where the turbidity trend is reversed for the 0, 20, and 40% cholesterol samples. The point is that the increase in turbidity observed with apo A-I cannot be attributed directly to the mere presence of cholesterol, as might be otherwise suspected.

Binding Coefficient (K_B) Determination. We define a binding coefficient as the fraction of total apo A-I that is bound to the vesicles

$$K_B = C_{bound}/C_{total} \quad (3)$$

where C_{bound} is the concentration of apo A-I that is bound to the vesicles and C_{total} is the total concentration of apo A-I. Presuming that shielding ensues until the surface area of DAG in the bilayer exceeds that of bound apo A-I, one would expect to observe rapid aggregation or a microstructural transition to complexes and DAG droplets when the DAG/bound apo A-I molar ratio exceeds 100 (that is, the ratio of molecular surface areas). The fact that cholesterol-free systems showed essentially no increase in turbidity for DAG/total apo A-I concentrations up to 109 (*11*) suggests that K_B is near unity in the absence of cholesterol. We therefore set $K_B = 1$ at 0 mol % cholesterol in this work and determine values for K_B for 20, 40, 50, and 60 mol % cholesterol as follows.

The enzyme kinetics model above is used to determine DAG concentration as a function of time for all cholesterol mole fractions. Careful inspection of Figure 4 shows that in cholesterol-free vesicles the turbidity is larger by a factor of approximately 6, when the DAG/total apo A-I molar ratio reaches 100, than the initial value. We therefore set a 6-fold

Table 1: Binding Coefficient (K_B) of Apo A-I

percent sterol	K_B	percent sterol	K_B
0	1	50	0.1383
20	0.8615	60	0.138
40	0.7533		

Table 2: DAG/Bound Apo A-I Molar Ratios as a Function of Time and Vesicle Composition (0.815 mM Total Lipid Concentration, 0.2 Unit of PLC, 89 μg/mL Apo A-I)

	cholesterol mole percentage				
time (h)	0%	20%	40%	50%	60%
0	0	0	0	1	1
0.5	53	52	47	218	180
1	89	88	79	372	307
1.5	112	111	101	473	392
2	126	125	115	540	449
8	145	148	140	674	573

increase in turbidity as the criterion for the time at which the DAG/bound apo A-I molar ratio reaches 100 (that is, when shielding is lost), irrespective of cholesterol composition, and use Figure 4 to identify when this criterion is met. The concentration of DAG at this time is known via the enzyme kinetics model, and the concentration of bound apo A-I is calculated by setting the DAG/bound apo A-I molar ratio equal to 100. A value for K_B is then determined from the total apo A-I concentration set by the experiment using eq 3. Values of K_B determined in this way are tabulated (see Table 1).

Predictions Based on K_B Values. The K_B values of Table 1, along with the PLC kinetics model, were used to calculate the molar ratio of DAG to bound apo A-I as a function of time in SUVs of varying cholesterol mole fraction at a PLC concentration of 0.2 unit and an apo A-I concentration of 89 μg/mL. Results, which are shown in Table 2, reveal the approximate times at which the DAG/bound apo A-I molar ratio exceeds 100. These are the same times at which one would expect shielding of DAG by bound apo A-I to be lost and so serve as predictions of times at which one would expect a sudden upturn in turbidity.

Observed SUV Aggregation Profile at a High (89 μg/mL) Apo A-I Concentration. Figure 5 shows the turbidity profiles of SUVs of varying compositions exposed to PLC and apo A-I simultaneously. Aliquots (3 mL) of SUVs of varying cholesterol mole percentages were exposed to 0.2 unit of PLC and 89 μg/mL apo A-I. Apo A-I completely suppresses SUV aggregation for only the 0 and 20 cholesterol mole percentages. The 40 mol % SUVs show a loss of suppression at 1.5 h. The 50 and 60% SUVs do not exhibit any suppression in absorbance.

PLC Quenching Studies. Cholesterol-free lecithin-only SUVs (0.652 mM total lipid) were exposed to PLC and apo A-I (51 μg/mL) in Figure 6. Of the two aliquots containing both apo A-I and PLC, one was "quenched" at 3 min with calcium-chelating agent EDTA to deactivate PLC. This quenched aliquot did not exhibit an increase in turbidity, whereas an unquenched aliquot exhibited an increase in turbidity beginning at 0.65 h. A comparison with the inset figure, which shows the DAG/apo A-I molar ratio as a function of time, reveals that the onset of an increase in turbidity corresponds very closely to the time (0.65 h) at which the DAG/apo A-I molar ratio exceeds 100.

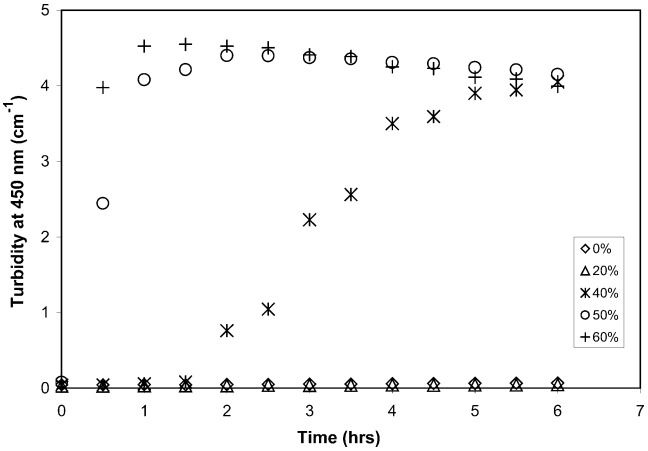

FIGURE 5: Effect of vesicle composition on the turbidity profile of SUVs at a high apo A-I concentration (89 μg/mL). A total of 0.2 unit of PLC and 89 μg/mL apo A-I were added to SUVs (0.815 mM total lipid concentration) of varying cholesterol contents. As in the low apo A-I case from Figure 4, higher cholesterol mole percentages yield higher turbidity values. SUV aggregation is completely suppressed in the 0% (◇) and 20% (△) samples. In the 40% (*) sample, aggregation is suppressed for about 1.5 h.

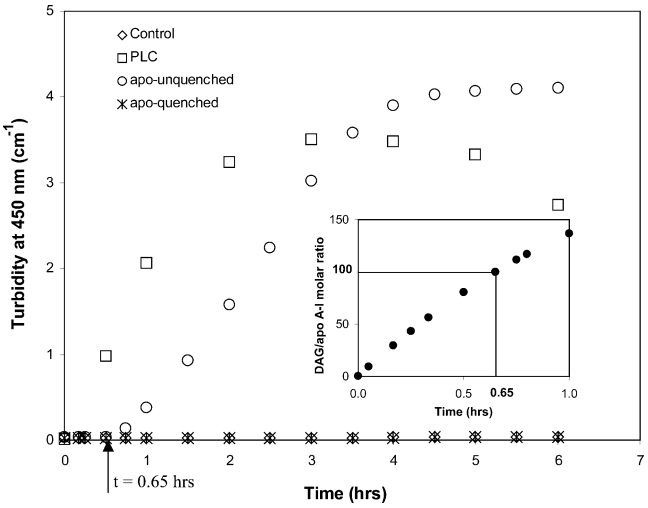

FIGURE 6: Effect of quenching of PLC (enzyme) action. All of the samples contained 0.652 mM lecithin-only vesicles. A total of 0.2 unit of PLC was added to all of the samples except the control sample. A total of 51 μg/mL apo A-I was present in the unquenched (○) and quenched (*) samples. EDTA was added at 3 min to quench the PLC action. Quenching of PLC with EDTA prevents the rise in turbidity that is observed in the unquenched sample. The inset shows the DAG/apo A-I molar ratio as a function of time. The time of increase in turbidity (0.65 h) closely corresponds to the time at which the DAG/apo A-I ratio exceeds 100. At 3 min, the time of quenching, DAG/apo A-I molar ratio is 9, which is below the critical value of 100.

Cryo-TEM Results. Figure 7 shows cryo-TEM images of quenched (a) and unquenched (b) aliquots from an independent experiment with conditions matching those of Figure 6. Round, typically unilamellar vesicles of 50−250 nm in diameter were seen in the quenched sample, with most vesicles of diameters around 150 nm. In the unquenched sample, oil droplets of up to 600 nm were identified. The polydispersity observed in the quenched sample is typical of sonicated vesicle dispersions; there are primarily unilamellar vesicles in the range stated above but also some that are very small (~30 nm) and a few quite large (~1 μm), as well as an occasional multilamellar vesicle. The un-

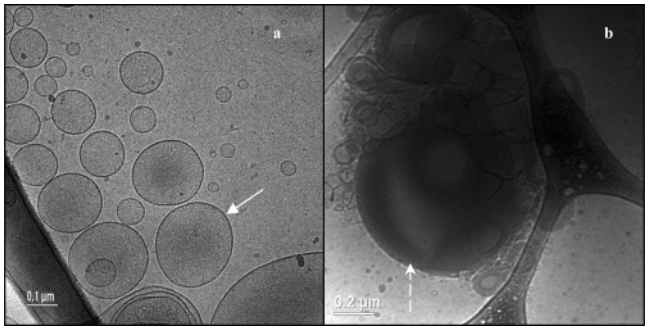

FIGURE 7: Cryo-TEM images of quenched (a) and unquenched (b) samples. Round, typically unilamellar vesicles of 50−250 nm in diameter were seen in the quenched sample, with most vesicles of diameters around 150 nm. In the unquenched sample, oil droplets of up to 600 nm were identified.

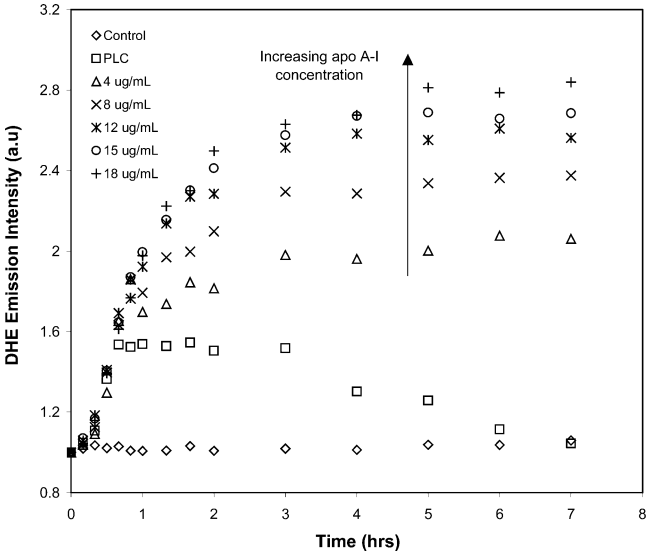

FIGURE 8: DHE fluorescence profiles of cholesterol-enriched (60 mol % sterol) SUVs. The SUVs (total lipid concentration of 6.51 mM) were labeled with 0.68 mM DHE. A total 0.4 unit of PLC was present in all except the control aliquot. The "PLC" (□) sample contained PLC alone. The rest of the samples contained PLC plus the apo A-I concentrations indicated in μg/mL. When present alone, PLC induced an increase in the DHE fluorescence for about 1 h after which a decrease in fluorescence intensity is observed. The presence of apo A-I in conjunction with PLC results in an increase in DHE fluorescence intensity that is higher than observed with PLC alone. The increase in DHE fluorescence intensity is directly proportional to the concentration of apo A-I present. The sample with the highest apo A-I concentration (18 μg/mL) experienced the maximum increase in DHE fluorescence intensity.

quenched sample, on the other hand, contains mostly oil droplets; a typical droplet is shown (Figure 7b).

DHE Fluorescence. Figure 8 depicts fluorescence profiles of cholesterol-enriched SUVs (60 mol % cholesterol, 6.51 mM total lipid concentration) labeled with 0.68 mM DHE. A total of 0.4 unit of PLC was present in all except the control, which contained neither apo A-I nor PLC. The control exhibits a constant DHE fluorescence intensity throughout the experiment. The DHE-labeled SUVs exhibit an apo A-I dose-dependent increase in DHE fluorescence intensity when both apo A-I and PLC are present. In this case, the sample with the highest apo A-I concentration (18 μg/mL) exhibits the highest DHE fluorescence intensity. When PLC is present alone, there is an increase in DHE fluorescence intensity for up to 1 h followed by a gradual decrease back to the initial (and control) value.

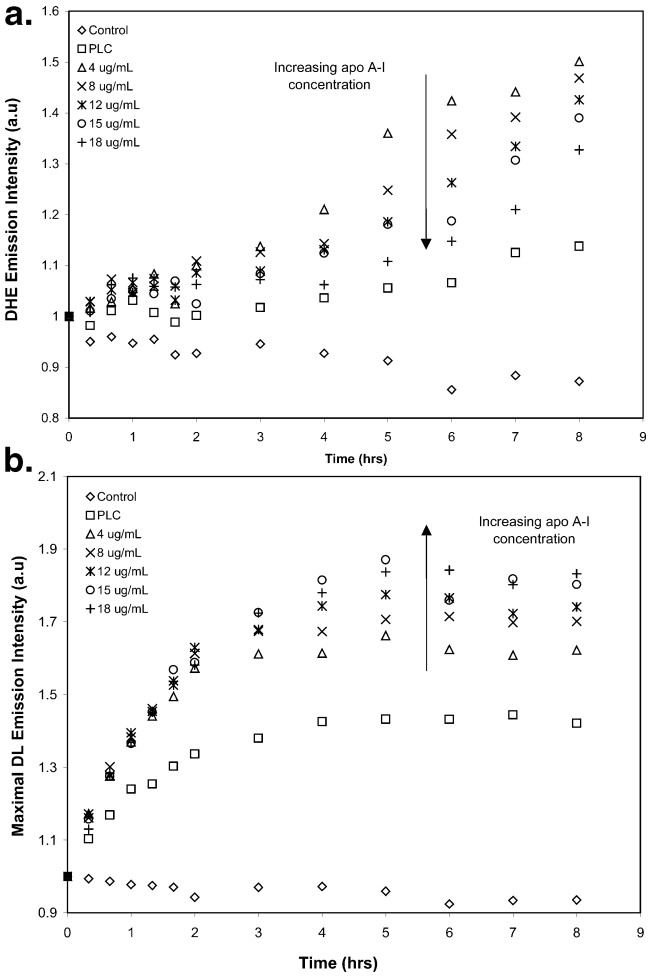

FIGURE 9: DHE to DL fluorescence resonance energy transfer. Cholesterol-enriched SUVs (60 mol % sterol) of total lipid concentration of 6.51 mM were labeled with 0.68 mM DHE and 0.078 mM DL. DHE (a) and DL (b) fluorescence intensities were plotted versus time for samples containing PLC alone (□) and PLC in conjunction with varying amounts of apo A-I (indicated in μg/mL). The control (◇) consisted of SUVs devoid of PLC and apo A-I. A total of 0.4 unit of PLC was present in all samples except the control. The presence of PLC induced an increase in both the DHE and DL fluorescence intensities. Apo A-I further enhanced the increase in the fluorescence intensity in both cases (DHE and DL). An apo A-I dose-dependent fluorescence behavior is observed. DHE fluorescence intensities decreased with increasing apo A-I concentrations, while the reverse trend was observed for DL fluorescence intensities. For the lowest apo A-I concentration employed (Δ, 4 μg/mL), DHE experienced the highest increase in fluorescence intensity, while DL experienced the lowest increase in fluorescence intensity. The opposite trend is seen for the highest (+, 18 μg/mL) apo A-I concentration employed.

DHE-to-DL FRET. Figure 9 depicts (a) DHE and (b) DL fluorescence profiles of cholesterol-enriched SUVs (60 mol % cholesterol, 6.51 mM total lipid concentration) labeled with both 0.68 mM DHE and 0.078 mM DL. A total of 0.4 unit of PLC was present in all except the control.

As for the case with DHE alone (Figure 8), the DHE- and DL-labeled SUVs also exhibit an apo A-I dose-dependent change in DHE fluorescence intensity when both apo A-I and PLC are present. However, in this case, the trend is reversed; that is, DHE fluorescence intensity decreases with increasing apo A-I concentration (see downward arrow in

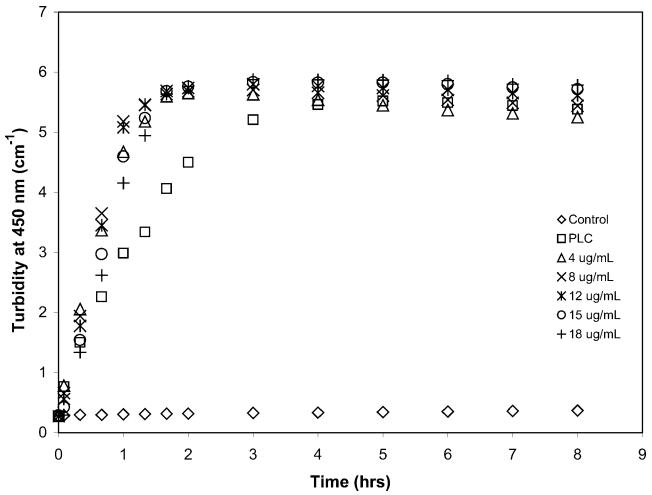

FIGURE 10: Turbidity of 60% sterol SUVs (6.51 mM total lipid concentration) labeled with DHE (0.68 mM) and DL (0.078 mM). Neither PLC nor apo A-I were present in the control (◇). A total of 0.4 unit PLC was added to all of the samples except the control. Apo A-I of the indicated concentration (in μg/mL) was added to all of the samples except the control and "PLC". The turbidity of the control was steady as a function of time. PLC induced an increase in turbidity, which plateaus after 4 h. Up to 1 h, an apo A-I dose-dependent suppression of turbidity was observed. After 1 h, the presence of apo A-I results in a turbidity value that is higher than seen in the "PLC" sample.

Figure 9a). At the same time, the DL fluorescence intensity increases with an increasing apo A-I concentration (see upward arrow in Figure 9b). The decrease in DHE intensity (Figure 9a) and the concomitant increase in DL intensity (Figure 9b) are similar in magnitude, suggestive of enhanced energy transfer from DHE to DL with increasing apo A-I.

Turbidity Profiles. Figure 10 shows turbidity profiles for cholesterol-enriched SUVs (60 mol % cholesterol, 6.51 mM total lipid concentration) containing both DHE and DL. A total of 0.4 unit of PLC was present in all except the control. The "PLC" sample contained PLC alone, and the remainder (except the control) contained PLC with apo A-I of varying concentrations shown in μg/mL. At earlier times (up to 1 h), higher apo A-I concentrations give lower turbidity values, in a reverse, dose-dependent fashion. At later times, the reverse trend is observed, with higher apo A-I concentrations giving higher turbidity values, in a direct, dose-dependent fashion.

DISCUSSION

This study focuses on the interplay between PLC and apo A-I in solutions of model bile. Previous work (*11*) revealed that apo A-I inhibits PLC-induced aggregation of cholesterol-free vesicles but that inhibition of cholesterol-rich vesicle aggregation is temporary. Eventually, large DAG oil droplets arise from the cholesterol-rich vesicles that coexist with small lecithin/cholesterol/apo A-I complexes. We hypothesized that the microstructural transition was not unique to cholesterol-rich vesicles but rather is a general phenomenon that depends on the relative amounts of apo A-I bound to the vesicles and DAG generated by PLC hydrolysis. The purpose of this work was to test this hypothesis by varying systematically both cholesterol composition and apo A-I concentration.

We investigated the behavior of cholesterol-enriched (60% sterol) and cholesterol-free (0% sterol) vesicles in the presence of a fixed PLC concentration and a range of (2−84 μg/mL) apo A-I concentrations. The total lipid concentration was fixed at 0.815 mM; thus, the substrate (lecithin) concentration was higher in the cholesterol-free system. With all other factors aside, one would then expect cholesterol-free SUVs to give the greatest extent of PLC-induced aggregation (as in the absence of apo A-I, Figure 3). This was not the case. For example, at the highest apo A-I concentration, (DAG-driven) vesicle aggregation was completely suppressed in the cholesterol-free system (Figure 2) but not in the cholesterol-enriched system (Figure 1), despite the fact that the amount of DAG at any particular time was higher in the cholesterol-free system than in the cholesterol-rich system.

We believe this seemingly paradoxical behavior is easily explained because cholesterol impedes apo A-I intercalation into phospholipid bilayers (*33*). Cholesterol-rich vesicles therefore have less bound apo A-I available to shield exposed DAG moieties against exposure to water. Apo A-I binding was quantified in terms of binding coefficients, K_B (Table 1), based on turbidity profiles observed at a relatively low apo A-I concentration of 19 μg/mL (Figure 4). Because predictions based on these K_B values would necessarily give good agreement with experimental data at the apo A-I concentration on which they were based, an independent test was performed to compare predictions with experimental results at a higher apo A-I concentration.

K_B values from Table 1 were used, in conjunction with an enzyme kinetics model, to track the DAG/bound apo A-I molar ratio as a function of time at an apo A-I concentration of 89 μg/mL (Table 2). On the basis of the premise that shielding is lost when the DAG/bound apo A-I molar ratio exceeds 100 (that is, ratio of molecular surface areas), one would expect turbidity to increase between 0 and 0.5 h at cholesterol mole percentages of 50 and 60% and to increase at ~1.5 h at a cholesterol mole percentage of 40%. Inspection of Figure 5, which depicts the measured behavior, reveals excellent agreement with these predictions. Following similar logic, one would expect the turbidity to rise between 1 and 1.5 h at cholesterol mole percentages of 0 and 20%, yet no such increase was observed. This suggests that the binding coefficients obtained at the lower cholesterol mole percentages do not capture all of the physics at play. For example, cholesterol exerts a well-known condensing effect on the lipid bilayer at cholesterol contents exceeding 20 mol % (*39*). Thus, in addition to differences in absolute binding to the vesicle, cholesterol might also alter somewhat the relative amount of DAG that can be shielded by a given amount of bound apo A-I. Coincident with the condensation effect is the formation of liquid-ordered domains, akin to rafts in cell-based systems (*40*−*42*). DAG is known to displace cholesterol from rafts, which is another complicating factor when cholesterol is present at greater than 20 mol %. Of course, it is possible that the critical DAG/bound apo A-I value is greater than 100, but this would still not account for the differences seen at 0 and 20 mol % cholesterol.

To further examine the extent to which DAG/bound apo A-I molar ratios determine SUV aggregation behavior, we performed PLC (enzyme) quenching studies (Figure 6). When EDTA (quencher) was added to a sample containing apo A-I and PLC at an early time (3 min), SUV aggregation was completely suppressed for the duration of the experi-

ment. An unquenched, control sample showed the typical rise in turbidity, commencing between 0.5 and 0.65 h. The DAG/bound apo A-I molar ratios at 3 min (quenching time) and 0.65 h (loss of suppression) were 9 and 100, respectively, confirming that the DAG/bound apo A-I molar ratio is a key parameter that determines the molecular events unfolding in the presence of PLC and apo A-I.

Cryo-TEM results further confirm suppression of SUV aggregation when the quencher was employed (Figure 7). In the unquenched sample, DAG oil droplets were present that resulted from a microstructural transition when the critical value (∼100) was exceeded. No such large structures were evident in the quenched sample, which contained vesicles primarily in the range of 50−250 nm.

Fluorescence studies aid in tracking molecular events as a function of time. We utilized fluorescent analogues of cholesterol and lecithin, DHE and DL, respectively, to monitor the lipid behavior. The presence of apo A-I induced an increase in the DHE fluorescence intensity above that observed in the presence of PLC alone for all conditions studied (Figure 8). The increase in fluorescence intensity is a result of DAG formation and a concomitant rise in the quantum yield of the fluorescent probe. The similarity of DHE fluorescence profiles at early times, irrespective of the apo A-I concentration, is confirmation that apo A-I does not interfere with PLC hydrolysis of lecithin. Eventually, vesicle aggregation leads to a decrease in DHE fluorescence intensity. Apo A-I shielding, which suppresses vesicle aggregation, also inhibits this decrease in fluorescence intensity.

In addition to its use as an individual fluorescence label, it is interesting to observe the fluorescence intensity of DHE in the presence of DL. DHE and DL form a FRET pair, and the two probes show changes in intensity with the apo A-I concentration that are similar in magnitude but opposite in sign. The enhancement of DL intensity at the expense of DHE intensity is clear evidence of enhanced energy transfer (from DHE to DL) with increasing apo A-I. This is consistent with a partitioning of the probes into small complexes that lack DAG and give rise to a smaller average separation between probes.

Thus, we have shown that the protective behavior of apo A-I against vesicle aggregation and cholesterol nucleation in the presence of PLC depends on the relative concentrations of lipids (cholesterol and lecithin) and proteins (apo A-I and PLC). The DAG/bound apo A-I molar ratio is the key parameter that drives this interaction. When this ratio is less than ∼100, apo A-I suppresses vesicle aggregation by shielding hydrophobic DAG moieties; when the ratio exceeds 100, cholesterol nucleation is avoided by a microstructural transition to DAG droplets and lecithin/cholesterol/apo A-I complexes. Although the findings are cast in the context of gallstone pathogenesis, it is likely that similar mechanisms are at play during atherosclerosis (for example, apo A-I protection against sphingomyelinase-induced aggregation of low-density lipoproteins).

ACKNOWLEDGMENT

We acknowledge the cryo-TEM assistance of Dr. Yamaira González (Department of Chemical Engineering, University of Delaware). This work was supported by a Transitional Funding Grant from The Whitaker Foundation.

REFERENCES

1. Wrenn, S. P., Kaler, E. W., and Lee, S. P. (1999) A fluorescence energy transfer study of lecithin-cholesterol vesicles in the presence of phospholipase C, *J. Lipid Res. 40*, 1483−1494.
2. Wrenn, S. P., Gudheti, M., Veleva, A. N., Kaler, E. W., and Lee, S. P. (2001) Characterization of model bile using fluorescence energy transfer from dehydroergosterol to dansylated lecithin, *J. Lipid Res. 42*, 923−934.
3. Holan, K. R., Holzbach, R. T., Hermann, R. E., Cooperman, A. M., and Claffey, W. J. (1979) Nucleation time: A key factor in the pathogenesis of cholesterol gallstone disease, *Gastroenterology 77*, 611−617.
4. LaMont, J. T., and Carey, M. C. (1992) Cholesterol gallstone formation. 2. Pathobiology and pathomechanics, *Prog. Liver Dis. 10*, 165−191.
5. Little, T. E., Madani, H., Lee, S. P., and Kaler, E. W. (1993) Lipid vesicle fusion induced by phospholipase C activity in model bile, *J. Lipid Res. 34*, 211−217.
6. Harvey, P. R. C., Upadhya, G. A., and Strasberg, S. M. (1991) Immunoglobulins as nucleating proteins in the gallbladder bile of patients with cholesterol gallstones, *J. Biol. Chem. 266*, 13996−14003.
7. Chijiiwa, K., Koga, A., Yamasaki, T., Shimada, K., Noshiro, H., and Nakayama, F. (1991) Fibronectin: A possible factor promoting cholesterol monohydrate crystallization in bile, *Biochim. Biophys. Acta 1086*, 44−48.
8. Groen, A. K. (1990) Nonmucous glycoproteins as pro-nucleating agents, *Hepatology 11*, 189S−194S.
9. Smith, B. F. (1987) Human gallbladder mucin binds biliary lipids and promotes cholesterol nucleation in model bile, *J. Lipid Res. 28*, 1088−1097.
10. Nùñez, L., Amigo, L., Rigotti, A., Puglielli, L., Mingrone, G., Greco, A. V., and Nervi, F. (1993) Cholesterol crystallization-promoting activity of aminopeptidase-N isolated from the vesicular carrier of biliary lipids, *FEBS Lett. 329*, 84−88.
11. Gudheti, M. V., Gonzalez, Y. I., Lee, S. P., and Wrenn, S. P. (2003) Interaction of apolipoprotein A-I with lecithin-cholesterol vesicles in the presence of phospholipase C, *Biochim. Biophys. Acta 1635*, 127−141.
12. Kibe, A., Holzbach, R. T., LaRusso, N. F., and Mao, S. J. T. (1984) Inhibition of cholesterol crystal formation by apolipoproteins in supersaturated model bile, *Science 225*, 514−516.
13. Tao, S., Tazuma, S., and Kajiyama, G. (1993) Apolipoprotein A-I stabilizes phospholipid lamellae and thus prolongs nucleation time in model bile systems: An ultrastructural study, *Biochim. Biophys. Acta 1166*, 25−30.
14. Carey, M. C. (1996) Formation and growth of cholesterol gallstones: The new synthesis, *Bile Acids: Cholestasis-Gallstones*; Fromm, H., Leuschner, U., Eds.; Kluwer, Dordrecht, The Netherlands.
15. Portincasa, P., van Erpecum, K. J., and Vanberge-Henegouwen, G. P. (1997) Cholesterol crystallization in bile, *Gut 41*, 138−141.
16. Strasberg, S. M. (1998) The pathogenesis of cholesterol gallstones—A review, *J. Gastrointest. Surg. 2*, 109−125.
17. Luk, A. S., Kaler, E. W., and Lee, S. P. (1993) Phospholipase C-induced aggregation and fusion of cholesterol-lecithin small unilamellar vesicles, *Biochemsitry 32*, 6965−6973.
18. Halpern, Z., Dudley, M. A., Kibe, A., Lynn, M. P., Breuer, A. C., and Holzbach, R. T. (1986) Rapid vesicle formation and aggregation in abnormal human biles: A time-lapse video-enhanced contrast microscopy study, *Gastroenterology 90*, 875−885.
19. Brown, D. A., and London, E. (1998) Structure and origin of ordered lipid domains in biological membranes, *J. Membr. Biol. 164*, 103−114.
20. Radhakrishnan, A., and McConnell, H. M. (1999) Condensed complexes of cholesterol and phospholipids, *Biophys. J. 77*, 1507−1517.
21. Troup, G. M., Tulenko, T. N., Lee, S. P., and Wrenn, S. P. (2003) Detection and characterization of laterally phase separated cholesterol domains in model lipid membranes, *Colloids Surf., B 29*, 217−231.
22. Troup, G. M., Tulenko, T. N., Lee, S. P., and Wrenn, S. P. (2003) Estimating the size of laterally phase separated cholesterol domains in model membranes with Förster resonance energy transfer: A simulation study, *Colloids Surf., B 33*, 57−65.

23. Troup, G. M., and Wrenn, S. P. (2004) Temperature and cholesterol composition-dependent behavior of 1-myristoyl-2-[12-[(5-dimethylamino-1-naphthalenesulfonyl)amino]dodecanoyl]-*sn*-glycero-3-phosphocholine in 1,2-dimyristoyl-*sn*-glycero-3-phosphocholine membranes, *Chem. Phys. Lipids 131*, 167−182.
24. Tulenko, T. N., Chen, M., Mason, P. E., and Mason, R. P. (1998) Physical effects of cholesterol on arterial smooth muscle membranes: Evidence of immiscible cholesterol domains and alterations in bilayer width during atherogenesis, *J. Lipid Res. 39*, 947−956.
25. Dass, C. R., and Jessup, W. (2000) Apolipoprotein A-I, cyclodextrins, and liposomes as potential drugs for the reversal of atherosclerosis: A review, *J. Pharm. Pharmacol. 52*, 731−761.
26. Kiss, R. S., Ryan, R. O., and Francis, G. A. (2001) Functional similarities of human and chicken apolipoprotein A-I: Dependence on secondary and tertiary rather than primary structure, *Biochim. Biophys. Acta 1531*, 251−259.
27. Jonas, A., Drengler, S. M., and Patterson, B. W. (1980) Two types of complexes formed by the interaction of apolipoprotein A-I with vesicles of L-α-dimyristoylphosphatidylcholine, *J. Biol. Chem. 255*, 2183-2189.
28. Li, H., Lyles, D. S., Thomas, M. J., Pan, W., and Sorci-Thomas, M. G. (2000) Structural determination of lipid-bound apo A-I using fluorescence resonance energy transfer, *J. Biol. Chem. 275*, 37048−37054.
29. Koppaka, V., Silvestro, L., Engler, J. A., Brouillette, C. G., and Axelsen, P. H. (1999) The structure of human lipoprotein A-I, *J. Biol. Chem. 274*, 14541−14544.
30. Pattinson, N. R. (1988) Identification of a phosphatidylcholine active phospholipase C in human gallbladder bile, *Biochem. Biophys. Res. Commun. 150*, 890−896.
31. Pattinson, N. R., and Willis, K. E. (1991) Effect of phospholipase C on cholesterol solubilization in model bile. A Concanavalin A-binding nucleation-promoting factor from human gallbladder bile, *Gastroenterology 101*, 1339−1344.
32. Busch, N., and Holzbach, R. T. (1990) Crystal growth-inhibiting proteins in bile, *Hepatology 12*, 195S−199S.
33. Tall, A. R., and Lange, Y. (1978) Interaction of cholesterol, phospholipid, and apopoprotein in high-density lipoprotein recombinants, *Biochim. Biophys. Acta 513*, 185−197.
34. Cabral, D., and Small, D. M. (1989) Physical chemistry of bile. In *Handbook of Physiology: The Gastrointestinal System III*; Schultz, S. G., Forte, J. G., Rauner, B. B., Eds; pp 621−662; American Physiological Society, Waverly Press, Baltimore, MD.
35. Lakowicz, J. R. (1999) *Principles of Fluorescence Spectroscopy*, 2nd ed.; Kluwer Academic/Plenum Publishers, New York.
36. Savitsky, A., and Golay, M. J. E. (1964) Smoothing and differentiation of data by simplified least squares procedures, *Anal. Chem. 36*, 1627−1639.
37. Bellare, J. R., Davis, H. T., Scriven, L. E., and Talmon, Y. (1988) Controlled environment vitrification system: An improved sample preparation technique, *J. Electron Microsc. Technol. 10*, 87−111.
38. Danino, D., Bernheim-Groswasser, A., and Talmon, Y. (2001) Digital cryogenic transmission electron microscopy: An advanced tool for direct imaging of complex fluids, *Colloids Surf., A 183*, 113−122.
39. Finegold, L. (1993) Cholesterol in membrane models, CRC Press, Boca Raton, FL.
40. Vist, M. R., and Davis, J. H. (1990) Phase equilibria of cholesterol/dipalmitoylphosphatidylcholine mixtures: Deuterium nuclear magnetic resonance and differential scanning calorimetry, *Biochemistry 29*, 451−464.
41. Brown, D. A., and London, E. (1998) Functions of lipid rafts in biological membranes, *Annu. Rev. Cell Dev. Biol. 14*, 111−136.
42. Loura, L. M. S., Fedorov, A., and Prieto, M. (2001) Fluid−fluid membrane micro heterogeneity: A fluorescence energy transfer study, *Biophys. J. 80*, 776−788.

BI047317M